

Flow Turbulence Combust (2007) 78:177–202  
DOI 10.1007/s10494-006-9067-x

---

# Compound Wall Treatment for RANS Computation of Complex Turbulent Flows and Heat Transfer

M. Popovac · K. Hanjalic

Received: 28 April 2006 / Accepted: 13 December 2006 /  
Published online: 18 January 2007  
© Springer Science + Business Media B.V. 2007

**Abstract** We present a generalised treatment of the wall boundary conditions for RANS computation of turbulent flows and heat transfer. The method blends the integration up to the wall (ItW) with the *generalised wall functions* (GWF) that include non-equilibrium effects. Wall boundary condition can thus be defined irrespective of whether the wall-nearest grid point lies within the viscous sublayer, in the buffer zone, or in the fully turbulent region. The computations with fine and coarse meshes of a steady and pulsating flow in a plane channel, in flow behind a backward-facing step and in a round impinging jet using the proposed *compound wall treatment* (CWT) are all in satisfactory agreement with the available experiments and DNS data. The method is recommended for computations of industrial flows in complex domains where it is difficult to generate a computational grid that will satisfy a priori either the ItW or WF prerequisites.

**Key words** RANS turbulence models · wall functions · integration to the wall · compound wall treatment

## 1 Introduction

The treatment of the wall boundary conditions has long been a stumbling block in computation of turbulent fluid flows, especially when accurate predictions of wall friction and heat transfer are the main targets. The problem is pertinent to the Reynolds-averaged Navier–Stokes (RANS) methods applied to complex flows, where the usually affordable computational grids are too coarse to permit integration of the governing equations up to the wall (ItW) and the use of the exact wall

---

M. Popovac (✉) · K. Hanjalic  
Department of Multi-scale Physics, Faculty of Applied Sciences,  
Delft University of Technology, Lorentzweg 1,  
2628 CJ Delft, The Netherlands  
e-mail: M.Popovac@tudelft.nl

boundary conditions. The same problem arises in large-eddy-simulations (LES) of high-Re-number wall-bounded flows where proper resolving of the near-wall flow regions requires extremely dense grids and excessive computational resources.

Integration up to the wall has not been very popular among industrial users of Computational Fluid Dynamics (CFD), except in some branches, e.g. aeronautics where, partly because of usually relatively simple geometries and, more importantly, because of high demands on accuracy, most simulations employ a near wall (“low-Re-number”) model. Such an approach requires models that account for wall-vicinity and viscous effects, thus a dense computational grid clustered in the wall-normal direction so that the first near-wall cell-centre is located at  $y^+ \mathcal{O}(1)$ . The common practice is to introduce “damping functions” in terms of non-dimensional wall distance or local turbulence Reynolds number in order to modify the eddy viscosity and some terms in the model equations by which to account for different, viscous and inviscid (wall blocking), near-wall effects. It has been known, however, that no pointwise damping functions – irrespective of their formulation and complexity – can account universally for physically very different effects such as the isotropic viscous damping of *all* turbulence fluctuations, and the non-isotropic (wall-configuration-dependent) non-viscous suppression of the wall-normal velocity fluctuations due to wall impermeability. Moreover, damping functions introduce usually additional non-linearity and often numerical stiffness, which, together with the unavoidable dense clustering of the computational grid (at least in the wall-normal direction), may lead to excessive computational costs. Admittedly, these shortcomings are model-dependent and more pronounced in the widely used  $k - \varepsilon$  than in the  $k - \omega$  or one-equation model families.

Another problem, often encountered in industrial computations of complex flows, especially with automatic gridding, is the difficulty in achieving the desired grid clustering and thus fulfilling a priori the fine-grid prerequisite in the *whole* flow domain. This is in particular the case with flow bounded with walls of complex topology, involving curvature, protrusions, cavities or other geometrical irregularities.

It has long been known that the more popular wall function approach (WF) that bridges the near-wall viscous layer tolerates much coarser grids, but here the first cell-centre ought to lie outside the viscosity affected region, roughly at  $y^+ \geq 30$ , which is also difficult to ensure in all regions in complex flows. Besides, the conventional WFs are often inadequate for computing complex flows of industrial relevance because they have been derived for simple wall-attached near-equilibrium flows with a number of presumptions that are valid only in such flows.

The continuous increase in computing power has resulted – among others – in a trend towards using denser computational grids for computing industrial flows. However, because of prohibitive costs, in most cases such grids are still too coarse to satisfy the prerequisites for the ItW. Instead, the first grid point often lies in the buffer layer ( $5 \leq y^+ < 30$  in the wall attached flows), making neither ItW nor WF applicable.

Recently, several proposals appeared in the literature aimed at improving and generalising the wall treatment. One can distinguish two approaches. The first approach, based on early ideas of Chieng and Launder [1] pursues to derive wall functions by splitting the first near-wall cell into a viscosity-affected sublayer and the fully turbulent part, then assuming the variation of all flow properties in each part of the cell and integrating the expressions over the complete cell. A more general

variant of such an approach are the so called Analytical Wall Functions of Craft et al. [2]. These authors abandoned most of the common near-equilibrium assumptions and derived the wall functions on the basis of the assumed eddy-viscosity distribution across the first near-wall cell. The second approach employs a blending between the wall-limiting and fully turbulent expressions for various flow properties in question, using blending functions that ensure a smooth transition between the two layers. This makes it possible to provide adequate conditions for the first near-wall grid node even if it lies in the buffer region. For example, Esch and Menter [4] proposed a quadratic blending of the wall-limiting (viscous) and the outer (turbulent) values of the shear-stress and of  $\omega$  to provide boundary conditions in their  $k$ - $\omega$  model with the wall functions. Other approaches have also been proposed. Assuming wall layer universality, Kalitzin et al. [5] proposed analytical or numerical pre-integration of the Couette-form model equations in the viscous sublayer for each turbulence model, claiming thus to ensure the consistency with the outer flow equations. They integrated the sublayer equations for a zero-pressure-gradient boundary layer for several popular turbulence models and stored results – normalised with the conventional inner-wall scaling (friction velocity and viscosity) – in form of look-up tables, which, combined with the standard log-law are recommended to be used to define boundary conditions. In a more sophisticated approach, Craft et al. [6] proposed to integrate the parabolised transport equations over an embedded fine grid within the first grid cell. Despite obvious improvements demonstrated in several test flows, the latter, as well as some other advanced treatments, have not always met with enthusiasm among the industrial users, possibly because of the model apparent complexity, non-trivial effort required for their incorporation into the existing CFD codes and – in some cases – encountered impediment of the computational robustness.

We present here a *compound wall treatment* (CWT), which reduces either to the ItW when the first near-wall cell is in the viscous sublayer, or to the appropriate WF when it lies in the fully turbulent region. When the first grid node is in the buffer region, the boundary conditions are provided from blending the viscous and fully turbulent limits using exponential blending functions. This blending is based on a generalisation of the expressions for the mean velocity and temperature profiles of Kader [7] that approximate reasonably well the whole wall region of a boundary layer, including its viscous/conductive and turbulent logarithmic layers. While other universal expressions can be found in the literature, which provide even better approximation for equilibrium boundary layers, especially in the buffer zone, the Kader's blending was adopted because it makes it possible to use the same blending functions for almost all relevant flow and turbulence properties in the same manner. It makes the model insensitive to the precise positioning of the first grid point and – within reasonable limits – to the quality of the mesh in the near-wall region. The CWT can be applied in conjunction with *any turbulence model* that permits integration to the wall with *any wall functions*. However, it is advisable to use a well-tuned, physically well-justified and robust ItW model, preferably without empirical damping functions, which has been proved to successfully reproduce properties of a minimum set of generic flows exhibiting various non-equilibrium effects (strong pressure gradients, separation, impingement, and others). Here we use the robust elliptic relaxation  $\zeta$ - $f$  model proposed by Hanjalić et al. [8] for the ItW. Likewise, no compound treatment will lead to success in computing non-equilibrium wall bounded flows with a relatively coarse grid, if the conventional wall functions

are used. For that reasons, we also present the newly developed *generalised wall functions* (GWF) that account for non-equilibrium effects and yet preserve the simple standard form making its implementation into the existing CFD codes very easy and straightforward. It is noted that the GWF formulation proposed here is applicable to any high-Re-number model, ranging from the standard  $k-\varepsilon$  to the second-moment (Reynolds stress) closures. Of course, depending on the model used, the stress components appearing in the wall functions will be evaluated either from the kinetic energy or from the corresponding eddy-viscosity expression, or from the solution of the (algebraic or differential) stress providing equation.

We begin with a brief outline of the  $\zeta-f$  ItW model, and then present the rationale and the outcome of the generalisation of the conventional wall functions (GWF) to account for the non-equilibrium effects through inclusion of the pressure gradient and convection. We then present the strategy of merging the two approaches into a unique compound wall treatment (CWT) and provide illustration of the method performance in a series of generic test flows.

## 2 The $\zeta-f$ Model for ItW

We point out first that any generalised or hybrid treatment of wall boundary conditions requires to use a turbulence model that allows integration to the wall, with incorporated molecular and wall-blocking modifications. This should ensure that the wall-vicinity effects are accounted for when the first grid node lies within the molecular sublayer or in the buffer zone. In principle, any near-wall (“low-Re-number”) model can be used, but we opted for the  $\zeta-f$  model [8], believed to be a good compromise between the model simplicity and its performance in capturing near-wall phenomena in complex flows. This model is in essence a variant of Durbin elliptic relaxation  $\overline{v^2}-f$  model [9], but with the eddy viscosity defined as  $\nu_t = C_\mu^\zeta \zeta k^2/\varepsilon$ , where  $\zeta = \overline{v^2}/k$  can be interpreted as the ratio of the wall-normal and the general (scalar) turbulence time scales,  $\tau_v = \overline{v^2}/\varepsilon$  and  $\tau = k/\varepsilon$ . The coefficient  $C_\mu^\zeta = 0.22$  is the same as used by Durbin, and comes from the requirement of equal eddy viscosity in the  $\zeta-f$  model and in the standard  $k-\varepsilon$  model in an equilibrium logarithmic layer where  $\zeta \approx 0.4$ . A model transport equation is solved for  $\zeta$  (derived from the original equations for  $\overline{v^2}$  and  $k$ , with some approximations) instead for  $\overline{v^2}$ . The elliptic relaxation effect is ensured by an equation for the elliptic relaxation function  $f$ , here derived with the quasi-linear pressure-strain model of Speziale et al. [10] (SSG) (for details see [8]<sup>1</sup>). The model is closed with the conventional model equations for  $k$  and  $\varepsilon$ . The complete set of the model equations read:

$$\nu_t = C_\mu^\zeta \zeta k \tau \quad (1)$$

$$\frac{D\zeta}{Dt} = f - \frac{\zeta}{k} \mathcal{P} + \frac{\partial}{\partial x_k} \left[ \left( \nu + \frac{\nu_t}{\sigma_\zeta} \right) \frac{\partial \zeta}{\partial x_k} \right] \quad (2)$$

<sup>1</sup>A similar model has also been independently proposed by Uribe and Laurence [11], but apart from the same basic idea of solving an equation for the  $\overline{v^2}/k$  ratio, the two models differ in many respects, [12].

$$L^2 \nabla^2 f - f = \frac{1}{\tau} \left( C_1 - 1 + C_2' \frac{\mathcal{P}}{\varepsilon} \right) \left( \zeta - \frac{2}{3} \right) \tag{3}$$

$$\frac{Dk}{Dt} = \mathcal{P} - \varepsilon + \frac{\partial}{\partial x_j} \left[ \left( \nu + \frac{\nu_t}{\sigma_k} \right) \frac{\partial k}{\partial x_j} \right] \tag{4}$$

$$\frac{D\varepsilon}{Dt} = \frac{(C_{\varepsilon 1} \mathcal{P} - C_{\varepsilon 2} \varepsilon)}{\tau} + \frac{\partial}{\partial x_j} \left[ \left( \nu + \frac{\nu_t}{\sigma_\varepsilon} \right) \frac{\partial \varepsilon}{\partial x_j} \right] \tag{5}$$

where the time and length scale are limited with the Kolmogorov scales as the lower bounds, and Durbin’s realisability constraints [13] providing the upper bounds:

$$\tau = \max \left[ \min \left( \frac{k}{\varepsilon}, \frac{a}{\sqrt{6} C_\mu^\zeta |S| \zeta} \right), C_\tau \left( \frac{\nu^3}{\varepsilon} \right)^{1/2} \right] \tag{6}$$

$$L = C_L \max \left[ \min \left( \frac{k^{3/2}}{\varepsilon}, \frac{k^{1/2}}{\sqrt{6} C_\mu^\zeta |S| \zeta} \right), C_\eta \left( \frac{\nu^3}{\varepsilon} \right)^{1/4} \right] \tag{7}$$

The coefficient  $a$  in (6), whose original recommended value  $a = 0.6$  follows from the definition of  $\zeta$ , plays the same role as  $C_L$  in (7).

Thus, the  $\zeta$ - $f$  model preserves the original elliptic relaxation concept of Durbin. It accounts separately for the non-viscous wall blocking via elliptic-relaxation (3), and for the viscous effects through the viscous diffusion and Kolmogorov time and length scales as the lower scale bounds. However, solving the  $\zeta$  instead of  $\overline{v^2}$  equation offers several important computational advantages:

- The source term in the  $\zeta$  equation contains the easily reproducible production of the turbulence kinetic energy  $\mathcal{P}$ , with the convenient zero value at the wall. This contrasts the  $\overline{v^2}$  equation where the source contains  $\varepsilon$  with a non-zero wall value, and which is notoriously difficult to reproduce accurately in the near-wall region.
- Close to a wall, the three terms on the right in the  $\overline{v^2}$  equation are all proportional to  $y^2$  – thus mutually in balance, whereas in the  $\zeta$  equation only  $f$  and  $\mathcal{D}\zeta$  (where  $\mathcal{D}$  denotes the diffusion term in (2)) have to be in balance because  $\mathcal{P}\zeta/k$  goes to zero faster than the other two. This is important especially when segregated solvers are used.
- The budget of the  $\zeta$  equation in the limit when the wall is approached provides the boundary condition for  $f$ :

$$f_w = \lim_{y \rightarrow 0} \frac{-2\nu\zeta}{y^2} \tag{8}$$

It is noted that the numerator and denominator in (8) vary as  $y^2$  as compared to  $y^4$  in the  $\overline{v^2}$ - $f$  model. This makes the boundary condition for  $f$  much less stiff, thus improving the computational robustness of the model. Expression (8) has also the same form as that for  $\varepsilon_w$  when expressed in terms of  $k$ , i.e.  $\varepsilon_w = \lim(2\nu k/y^2)_{y \rightarrow 0}$ , and, therefore, it can be treated in an analogous manner in the computational procedure.

The model coefficient, tuned in a set of generic flows [8], are listed in the table below:

$C_\mu^\zeta$	$C_{\varepsilon 1}$	$C_{\varepsilon 2}$	$C_1$	$C_2'$	$\sigma_k$	$\sigma_\varepsilon$	$\sigma_\zeta$	$C_\tau$	$C_L$	$C_\eta$
0.22	$1.4(1 + 0.012/\zeta)$	1.9	1.4	0.65	1	1.3	1.2	6.0	0.36	85

Because of more convenient boundary conditions for  $f$ , the  $\zeta$ - $f$  model proved to be more robust and less sensitive to near-wall gridding than its parent  $\bar{v}^2$ - $f$  model, tolerating the first grid point up to  $y^+ < \approx 3$ . It is noted that in the limit of isotropic turbulence  $\zeta \rightarrow 2/3$  and the  $\zeta$ - $f$  model reduces to the conventional  $k$ - $\varepsilon$  model. Thus, while undoubtedly improving the near-wall predictions, for complex flows with swirl, rotation, strong three-dimensionality and other non-equilibrium effects, which may generate strong stress anisotropy, one is still advised to switch to a second-moment (differential or algebraic) model with near-wall modifications, to serve as the base ItW model. However, it is stressed that the choice of the base ItW model does not affect the blending strategy of the compound wall treatment outlined bellow.

### 3 Generalised Wall Functions (GWF)

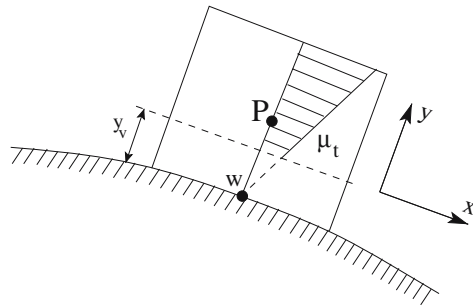
#### 3.1 Velocity field

When the first grid point is in the fully turbulent region, it is inevitable to use wall functions to provide the wall shear stress and other variables at the first near-wall grid node. The wall functions relate the values of the variables in the cell centres with those at the wall through pre-integrated simplified expressions, thus providing indirectly the wall boundary conditions. A compound wall treatment should automatically ensure this. However, the standard wall functions are known to fail in non-equilibrium flows because they have been derived using several assumptions: constant (turbulent) shear stress  $\bar{u}\bar{v}$ , proportional to the (also constant) turbulence kinetic energy  $k$  (so that  $\bar{u}\bar{v}/k \approx 0.3$ ), the semi-logarithmic mean velocity distribution, local energy equilibrium ( $\mathcal{P} = \varepsilon$ ), and a linear length-scale variation. In most flows of practical relevance none of these assumptions holds. In order to relax at least in part the above constraints, some authors included the pressure gradient to modify the conventional WFs. Such are the “non-equilibrium” WFs of Ng et al. [14] (available in FLUENT CFD code). We followed here the arguments of Craft et al. [2] and derived more general wall functions for the velocity and temperature, based on a single assumption that the non-dimensional eddy viscosity varies linearly with the distance from the wall, which was found to hold reasonably well even in strongly non-equilibrium flows. However, our assumed distribution differs from that of Craft et al.: instead of  $\mu_t = \rho\kappa u_\tau (y - y_v)$  (for  $y > y_v$ , where  $y_v$  is the assumed thickness of the viscous sublayer, to be determined empirically), we adopted a simpler formulation without including explicitly the viscous sublayer thickness  $y_v$ , Fig. 1:

$$\mu_t = \begin{cases} 0 & \text{for } y < y_v \\ \rho\kappa u_\tau y & \text{for } y \geq y_v \end{cases} \tag{9}$$

where  $\rho$  is the density,  $\kappa = 0.41$  is the Von Karman constant and  $u_\tau$  is the inner wall velocity scale (equal to the friction velocity  $\sqrt{\tau_w/\rho}$  in equilibrium wall flows).

**Fig. 1** Sketch of the near-wall cell with the assumed turbulent viscosity



While the above assumption for  $\mu_t$  may not hold universally, especially in and around singularities such as stagnation, separation and reattachment, it is reasonably general [15]. Admittedly, the discontinuity in the eddy viscosity distribution at  $y_v$  raises the question of consistency of the solutions in the inner (viscous) and outer (turbulent) wall layers, but this discontinuity is smoothed by imposing the continuity and smoothness of the velocity at the layers interface and smooth blending functions when compound wall treatment is applied, see below. Of course, we could have adopted a continuous and smooth  $\nu_t$  distribution in the sense of Van Driest, but this would lead to a much more complex integration. We point out that this  $\nu_t$  distribution is used only to derive the generalised wall functions for the fully turbulent region and not for integration of model equations over the complete wall layer. The major advantage of the present approach is that it leads to a simple formulation of the wall functions, compatible with the standard expressions, so that they can be easily implemented in the existing in-house or commercial CFD codes, as shown bellow.

We consider now the two-dimensional momentum equation for the wall-tangential direction, written for convenience as

$$\frac{\partial}{\partial y} \left[ (\mu + \mu_t) \frac{\partial U}{\partial y} \right] = C_U \tag{10}$$

with

$$C_U = \rho \frac{\partial U}{\partial t} + \rho U \frac{\partial U}{\partial x} + \rho V \frac{\partial U}{\partial y} + \frac{\partial p}{\partial x} \tag{11}$$

where  $t$  is the time,  $U$  and  $V$  are the velocity vector components in the wall-tangential and wall-normal direction respectively (denoted as  $x$  and  $y$  coordinates, as shown in Fig. 1) and  $p$  is the pressure.

With the above assumed  $\mu_t$ , (10) can be integrated twice over the two parts of the near-wall cell, provided we know  $C_U$ . Here we introduced an additional assumption that  $C_U$  can be taken as constant over the cell and known from the previous time step or iteration. A justification for this assumption is provided in Fig. 2 where the convection and pressure gradient, extracted from the  $\zeta-f$  ItW RANS computations, are plotted along the walls at several non-dimensional distances typical for the WF application ( $y^+ = 20, 40$  and  $60$ ) for flow behind a backward-facing step (including the separation bubble) and in a round impinging jet. All three lines in both (strongly non-equilibrium) flows show remarkable coincidence, justifying the assumption that  $C_U$  is reasonably constant over the cell.

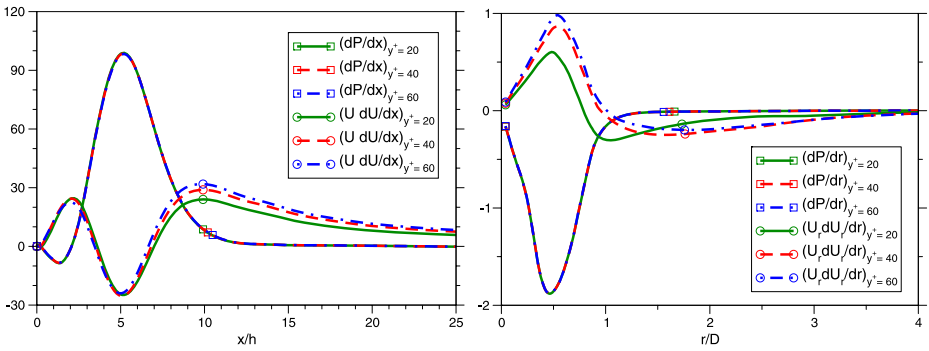


**Fig. 2** A priori analysis of the non-equilibrium effects in the wall vicinity for the backward-facing step flow (*left*) and the axisymmetric impinging jet (*right*)

The two constants, appearing after the double integration of (10) are deduced from the imposed conditions of continuity and smoothness of the velocity profile (equal values and gradients of  $U$  at the edge of the viscous sublayer  $y_v$ ), yielding (after some rearrangement) to an expression for the shear stress (with  $U$  and  $y$  corresponding to the cell-centre point):

$$\tau_w = \frac{\rho U - \frac{C_U y}{\kappa u_\tau}}{\frac{\rho y_v}{\mu} + \frac{\ln\left(\frac{y}{y_v}\right)}{\kappa u_\tau}} \tag{12}$$

When the near-wall cell is in the fully turbulent region, (12) serves for defining the velocity wall function.

### 3.1.1 Reduction to the conventional WF expressions

In order to arrive to practical expressions for the WF, preferably in the conventional recognisable form, thus making them easily implementable into the existing CFD codes, we consider first the behaviour of (12) and define  $y_v$ . The denominator of (12) is first rearranged as follows:

$$\frac{\rho y_v}{\mu} + \frac{\ln\left(\frac{y}{y_v}\right)}{\kappa u_\tau} = \frac{1}{\kappa u_\tau} \left[ \frac{\rho \kappa u_\tau y_v}{\mu} + \ln\left(\frac{y}{y_v}\right) \right] = \frac{1}{\kappa u_\tau} \ln\left(\frac{e^{\kappa y_v^+} y^+}{y_v^+}\right) = \frac{1}{\kappa u_\tau} \ln(E y^+) \tag{13}$$

By inserting the value for the viscous sublayer thickness  $y_v^+ = 11$ , which corresponds to the intersection of the linear and semi-logarithmic velocity laws, one gets  $e^{\kappa y_v^+} / y_v^+ = 8.3$ . This is the value of the additive constant  $E$  in the standard log-law, which in a sense explains the physical meaning of this constant.

In the nominator of (12) we extract the velocity, and treat jointly all the other terms:

$$U - \frac{C_U y}{\rho \kappa u_\tau} = U \left( 1 - \frac{C_U y}{\rho U \kappa u_\tau} \right) = U \psi \tag{14}$$

where

$$\psi = 1 - \frac{C_U y}{\rho U \kappa u_\tau} \tag{15}$$

We can now write the “non-equilibrium function” in a non-dimensional form as

$$\psi = 1 - \frac{C_U^+ y^+}{U^+ \kappa} \tag{16}$$

where  $y^+ = u_\tau y / \nu$ , and

$$C_U^+ = \frac{\nu}{\rho u_\tau^3} \left[ \rho \frac{\partial U}{\partial t} + \rho U \frac{\partial U}{\partial x} + \rho V \frac{\partial U}{\partial y} + \frac{\partial p}{\partial x} \right] \tag{17}$$

Finally, inserting (13) and (15) into (12) we get the new, generalised semi-logarithmic expression for the velocity distribution in the fully turbulent wall layer:

$$U^+ = \frac{1}{\kappa \psi} \ln(E y^+) \tag{18}$$

which is identical with the standard log-law, apart from the correction factor  $\psi$  that accounts for local non-equilibrium flow effects.

It is noted that in order to avoid singularity when  $u_\tau$  tends to zero, one should follow the conventional practice and replace  $u_\tau$  by

$$u_k = C_\mu^{1/4} k^{1/2} \tag{19}$$

The wall shear stress is evaluated in the same manner as in the conventional WF approach from the expression

$$\tau_w^t = \frac{\rho \kappa C_\mu^{1/4} k_P^{1/2} U_P}{\ln(E y_P^*)} \psi_P = \mu_w \frac{U_P}{y_P} \psi_P \tag{20}$$

where 
$$\mu_w = \frac{\kappa \rho C_\mu^{1/4} k_P^{1/2} y_P}{\ln(E y_P^*)} = \mu \frac{y_P^*}{U_P^*} \quad \psi_P = 1 - \frac{C_U y_P}{\rho \kappa C_\mu^{1/4} k_P^{1/2} U_P}$$

and 
$$U_P^* = \frac{1}{\kappa} \ln(E y_P^*) \quad y_P^* = \frac{C_\mu^{1/4} k_P^{1/2} y_P}{\nu} \tag{21}$$

$C_\mu = 0.07$ , the subscript “P” denotes the wall nearest cell-centre (see Fig. 1), and  $\psi_P$  includes via  $C_U$  the tangential pressure gradient and convection, thus accounting for local non-equilibrium effects.

As expected, for equilibrium flows ( $C_U = 0$  so  $\psi = 1$ ) (18) reduces to the standard log-law. The influence of the correction factor  $\psi$  in flows with non-equilibrium effects is a priori analysed by plotting (18) using the available experimental data or numerical solutions of several generic flows, such as a turbulent boundary layer

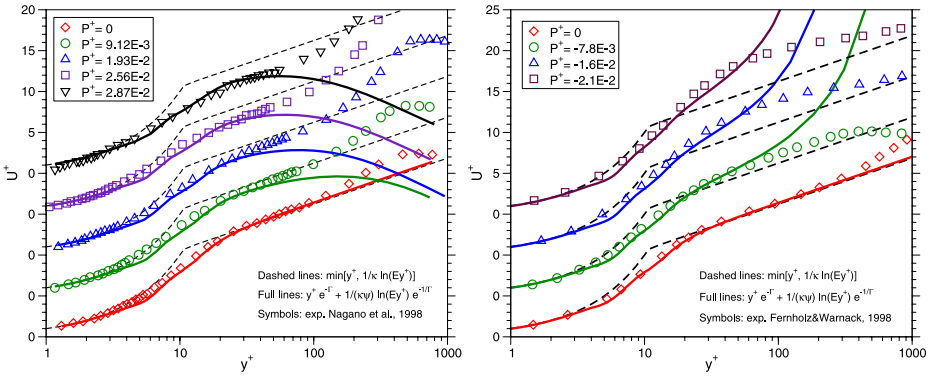


**Fig. 3** Boundary layer subjected to adverse (*left*) and favourable (*right*) pressure gradients; A priori test of GWF and CWT

subjected to strong adverse and favourable pressure gradients at different  $P^+ = \nu/\rho u_\tau^3 \partial p/\partial x$ , a flow behind a backward-facing step and a round impinging jet, Figs. 3, 4 and 5 respectively. The reader should focus at the moment only on the fully turbulent region ( $y^+ \geq 30$  in Fig. 3 and broken lines in Figs. 4 and 5). The latter two figures refer to the backward-facing step at  $Re = 28,000$  of Vogel and Eaton [25] and the axisymmetric impinging jet at  $Re = 23,000$  of Baughn and Schimizu [26]. The wall-tangential velocity has been recovered using (18). It is seen that the

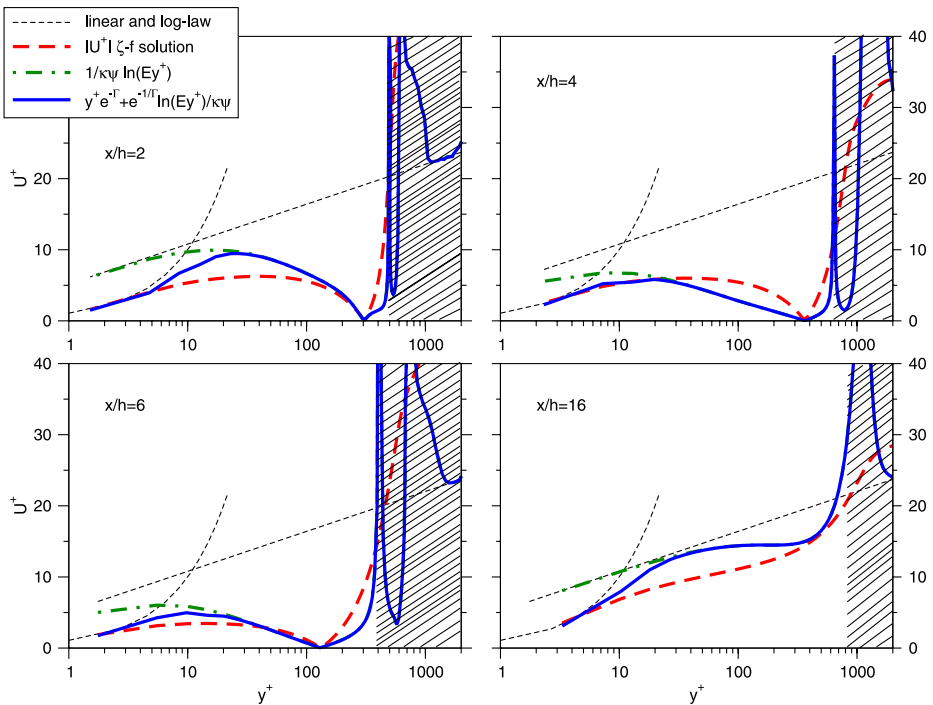


**Fig. 4** Backward-facing step flow,  $Re = 23,000$ ; A priori test of GWF and CWT

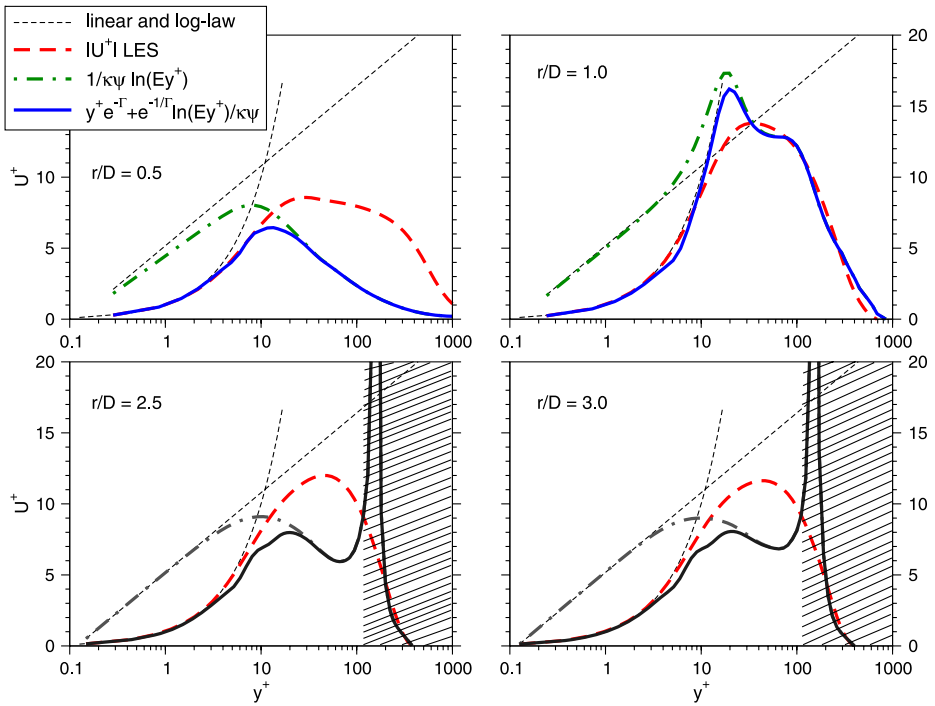


**Fig. 5** Axisymmetric impinging jet,  $Re = 23,000$ ; A priori test of GWF and CWT

balance between the convection and pressure gradient prevents an excessive growth of  $C_U$  unlike in boundary layers with strong pressure gradients, Fig. 3. However, in the region of very strong convection (hatched regions in Figs. 4 and 5), (18) is unsatisfactory because of effects that the expression does not account for. As shown in Fig. 6, the distributions of the wall-nearest cell-centre  $y_p^+$  for these two flows for several uniform grids, when projected to Figs. 4 and 5, indicate that (18) captures reasonably well the velocity with the first grid point being located in a wide range of  $y^+$  up to 400 in the backstep flow considered, whereas the impinging jet is

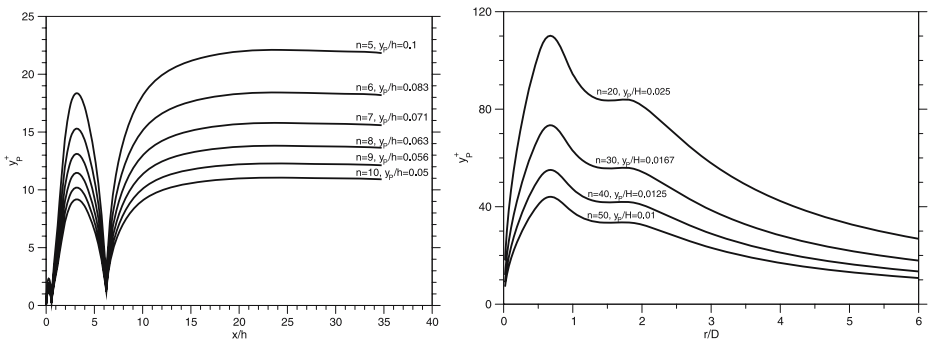


**Fig. 6** Distribution of the first near-wall cell-centre  $y_p^+$  for different (uniform) meshes. *Left*: a back-step flow at  $Re = 28,000$ ,  $n$  denotes the number of cells over the step height. *Right*: a round impinging jet at  $Re = 23,000$ ,  $n$  denotes the number of cells from jet exit to the impingement plate

less satisfactory for  $y_p^+ > 10$  but still much better than with the conventional Wall Functions. More discussion of these tests for the complete wall layer will be provided below in conjunction with the compound wall treatment.

### 3.2 Scalar field

One can follow the analogous approach and derive the generalised wall function for the temperature  $T$  (and other scalars, e.g. mass concentration) and include the effects of convection and of the source terms through an analogous  $\psi_T$  and  $C_T$  parameters. The resulting expression for the non-dimensional temperature variation can then be reformulated in terms of  $U^+$  given by (18), as practiced in the conventional WF and wall-scaling approach, yielding

$$\Theta^+ = \sigma_t \left[ \frac{\psi}{\psi_T} U^+ + J \left( \frac{\sigma}{\sigma_t} \right) \right] \tag{22}$$

where  $\sigma$  and  $\sigma_t$  are the molecular and turbulent Prandtl numbers respectively, and

$$\Theta^+ = \frac{(T_w - T) \rho c_p u_\tau}{q_w} \tag{23}$$

$$\psi_T = 1 - \frac{\sigma_t C_T y}{\kappa u_\tau \rho c_p (T - T_w)} \quad \text{and} \quad C_T = \rho c_p \left[ \frac{\partial T}{\partial t} + U \frac{\partial T}{\partial x} + V \frac{\partial T}{\partial y} \right] + \dot{q}_{int} \tag{24}$$

Here  $c_p$  denotes the specific heat capacity,  $q_w$  is the wall heat flux,  $\dot{q}_{int}$  denotes an internal heat source if any, and  $J$  is the viscous sublayer thermal resistance, commonly referred as the Jayatilleke “J-function” [3], for which several definitions can be found in the literature, and  $U^+$  is given by (18) that includes the non-equilibrium factor  $\psi$ .

In flows with significant effects of thermal (or mass) buoyancy, (22) can also be used, in which case  $C_U^+$  should also include the buoyancy force in the  $x$  direction  $\beta \rho g_x (T - T_0)$ , where  $\beta$  is the expansion factor. However, for passive scalars without an internal heat source and with a milder pressure variation one can assume that the time rate of change and convective transport of momentum and energy are similar, allowing to assume that  $\psi_T \approx \psi$ . This leads to the simpler conventional expression for the non-dimensional temperature in terms of the generalised velocity expression, i.e.

$$\Theta^+ = \sigma_t \left[ U^+ + J \left( \frac{\sigma}{\sigma_t} \right) \right] \tag{25}$$

### 4 Compound Wall Treatment (CWT)

We consider now a blending of the two approaches into a unified procedure that should provide the wall boundary conditions irrespective of whether the first near-wall grid node lies in viscous sublayer, turbulent zone, or in the buffer region in the between. The method should reduce to the one of the above two procedure (ItW or GWF) when the first grid node happens to lie in the region appropriate

to each approach. If the cell-centre lies in the buffer zone, the boundary conditions are again provided in the form of wall functions, but modified to account for the viscous/molecular and other (inviscid) wall effects.

The quantities for which the boundary conditions ought to be specified in the CWT depend, like in the conventional WF approach, on the turbulence model used. The primary variables are the wall shear stress  $\tau_w$  and its relation to the mean velocity, wall heat flux  $q_w$  and its relation to the mean temperature, the production  $\mathcal{P}$  and dissipation  $\varepsilon$  of the turbulence kinetic energy  $k$ . For the  $\zeta$ - $f$  model considered here we also need the wall function for the elliptic function  $f$ .

Earlier attempts to derive a unified wall treatment were based on a single expression adopted from the literature for the mean velocity throughout the whole boundary layer. A number of such expressions are available (e.g. Reichardt [16], Spalding [17], Musker [18], Liakopoulos [19]), which fit perfectly the experimental data from the the wall to the outer turbulent region in equilibrium wall boundary layers, but none of them is applicable to non-equilibrium situations. Other expressions were derived from curve-fitting, e.g. Shih et al. [20]. However, in addition to lacking any non-equilibrium effects, the disadvantage of using such expressions is that they were derived only for velocity (and, in some cases for temperature). This means that for other variables other empirical (curve-fitted) “unified” expressions ought to be invented, which proved to be difficult for general flows.

If the expressions for the wall-limited and for the outer turbulent values of the variables in question are known (or can be provided from e.g. GWF), we can merge these expressions by using a suitable blending. Esch and Menter [4] proposed to use the quadratic mean

$$\phi_P = \sqrt{\phi_\nu^2 + \phi_t^2} \tag{26}$$

where  $\phi$  is the variable considered, and the subscript  $\nu$  denotes the viscous (wall-limiting) and  $t$  the fully turbulent value of that variable.

This expression has no physical justification, but it does have the correct limiting behaviour: it reduces to the viscous or the fully turbulent value in their respective regions. This is illustrated in Fig. 7 by plotting for various  $y_p^+$  the a priori evaluated non-dimensional wall shear stress  $\tau_w$ , obtained from the above expressions for a plane channel flow at  $Re_\tau = 800$ , using the DNS data [21]. The viscous shear stress was

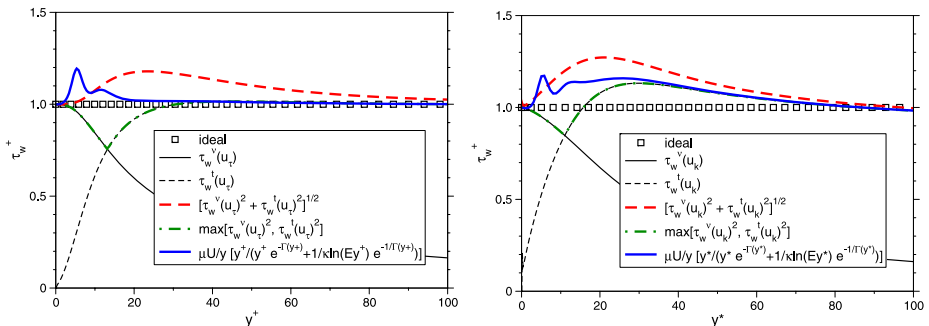


**Fig. 7** A priori evaluation of the blending expressions for  $\tau_w$ . *Left*: variables normalised with  $u_\tau$  (“+” normalisation). *Right*: variables normalised with  $u_\kappa$  (“\*” normalisation). Symbols: DNS of Tanahashi et al. [21]

evaluated using  $\tau_w^v = \mu U_P / y_P$ , while for the turbulent one we tested two definitions. The first was obtained from the log-law expression  $\tau_w^t = \rho [\kappa U_P / \ln(Ey_P^+)]^2$  using  $u_\tau = \sqrt{\tau_w / \rho}$  (“+” normalisation), and the second one, commonly practiced in all CFD codes is evaluated from  $\tau_w^t = \rho \kappa C_\mu^{1/4} k_P^{1/2} U_P / \ln(Ey_P^*)$  where  $u_k = C_\mu^{1/4} k^{1/2}$  (“\*” normalisation). The abscissa denotes the normalised distance of the first near-wall grid node “P”. The ideal model expressions should always give  $\tau_w^+ = 1$  irrespective of the grid-node location, which would be achieved if an expression for  $U^+$  was used that fits perfectly the complete region for  $0 < y^+ < y_\delta^+$  (e.g. [17] to [19]), where  $y_\delta^+$  is the limiting value of  $y^+$  beyond which the logarithmic law is no more valid. One can see that the viscous definition  $\tau_w^v$  reproduces the exact boundary value at the wall and it fits the DNS profile in the viscous sublayer up to approximately  $y^+ < 5$ , but diminishes fast towards zero further away. The fully turbulent definition  $\tau_w^t$  goes from very small value close to the wall to the proper value in the fully turbulent region, which, in this case is recovered only at about  $y^+ > 70$ . In the buffer region ( $5 < y^+ < 30$ ) both definitions give approximately the same values. The quadratic mean obtained from (26), produces higher values than the target  $\tau_w^+$ . This overestimation of  $\tau_w$  in the buffer region, but also in a part of the log-layer (up to  $y^+ \approx 80$  due to contamination by the viscous contribution), can produce significant errors in computing friction and heat transfer.

One can also generalise the expression (26) by using  $(\phi_v^n + \phi_t^n)^{1/n}$  to obtain better approximation in the buffer layer, but the author’s experience with  $n = 4$  produced only marginal improvement. In fact, it seems that using either of the two definitions alone is better approximation than their quadratic mean. This means that a simple switching formula could also be used to get the variable in the buffer region (especially for the variables like  $\varepsilon$ , which have a strong variation in the wall region):

$$\phi_P = \max(\phi_v, \phi_t) \tag{27}$$

A priori evaluation of (27) for the plane channel flow is also shown in Fig. 7 showing, just like (26), unsatisfactory result in the buffer region.

In order to achieve better reproduction in the buffer region one can combine the viscous and fully turbulent values by means of a suitably chosen smooth blending function in terms of some local flow quantities. We considered the blending of the wall-limiting and fully turbulent properties in the manner of Kader [7], who proposed a single expression for the temperature profile throughout the whole wall boundary layer:

$$\Theta^+ = Pr y^+ e^{-\Gamma_\Theta} + [\alpha \ln(y^+) + \beta(Pr)] e^{-1/\Gamma_\Theta} \tag{28}$$

where  $\alpha = 2.12$  and  $\beta(Pr) = (3.85 Pr^{1/3} - 1.3)^2 + 2.12 \ln(Pr)$  are the thermal-boundary-layer parameters, and the blending coefficient  $\Gamma_\Theta$  is a function of the normalised distance to the wall  $y^+ = u_\tau y / \nu$ , as follows:

$$\Gamma_\Theta = \frac{0.01 (Pr y^+)^4}{1 + 5 Pr^3 y^+} \tag{29}$$

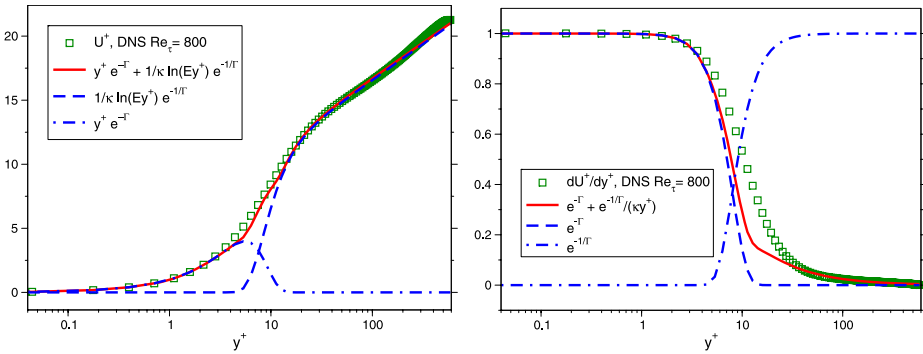


**Fig. 8** A priori evaluation of the expression (30) for the mean velocity and its wall-normal gradient, with indicated viscous and turbulent contributions. Symbols: DNS of Tanahashi et al. [21]

By simply inserting  $Pr = 1$ , (28) and (29) can be applied to the velocity profile:

$$U^+ = y^+ e^{-\Gamma} + \left[ \frac{1}{\kappa} \ln(Ey^+) \right] e^{-1/\Gamma} \tag{30}$$

$$\Gamma = \frac{0.01y^{+4}}{1 + 5y^+} \tag{31}$$

Expressions (28) and (30) define the blending of the viscous and the fully turbulent definition of  $\Theta^+$  and  $U^+$  through the blending functions  $e^{-\Gamma\Theta}$  and  $e^{-\Gamma}$  respectively.

Using (31), (30) is plotted in Fig. 8 showing acceptable agreement with the DNS results for a plane channel across the whole flow. The gradient  $dU^+/dy^+$  derived from (30), shown in the same figure, which is of interest for defining a wall function for the production of turbulent kinetic energy (see below), is more sensitive and deviates somewhat in the buffer region, but in view of other approximations, it can be considered also as acceptable.

Representing the CWT for the velocity, (30) is also tested a priori in the same generic cases as the GWF discussed above: in boundary layers subjected to strong adverse and favourable pressure gradients, Fig. 3, in a back-step flow, Fig. 4, and in a round impinging jet, Fig. 5 (chain line). These figures show that the first grid node can lie in a broad range of  $y^+$  ranging from the wall ( $y^+ = 0$ ) to a value well in the turbulent zone (depending on the flow type and Reynolds number,  $y^+ = 80 - 200$ ) producing in all cases acceptable agreement with the ItW solutions obtained on a fine grid (full line). For boundary layers subjected to strong pressure gradients, the agreement is excellent for  $0 < y^+ < 80$ . For other two test cases, at some flow cross-sections there are some deviations, but in all cases the CWT results (chain line) are much closer to the ItW solutions than the conventional WFs. Note that in the hatched zone of Figs. 4 and 5 the assumptions under which the WF expressions are derived are not valid any more.

We now apply this blending principle to all flow properties for which boundary conditions are required at the first near-wall grid node “P”, i.e.

$$\phi_P = \phi_v e^{-\Gamma} + \phi_t e^{-1/\Gamma} \tag{32}$$

The variables in play are primarily the wall shear stress  $\tau_w$ , kinetic-energy production  $\mathcal{P}$  and dissipation rate  $\varepsilon$ , and in the case of  $\zeta$ - $f$  model also for the elliptic function  $f$ .

**Wall shear stress** A straightforward application of (32) would lead to:

$$\begin{aligned} \tau_w &= \tau_w^v e^{-\Gamma} + \tau_w^t e^{-1/\Gamma} \\ &= \mu \frac{U_P}{y_P} e^{-\Gamma} + \frac{\rho \kappa C_\mu^{1/4} k_P^{1/2} U_P \psi_P}{\ln(Ey_P^*)} e^{-1/\Gamma} \\ &= (\mu e^{-\Gamma} + \mu_{w,P} \psi_P e^{-1/\Gamma}) \frac{U_P}{y_P} \end{aligned} \tag{33}$$

where  $\mu_w$  and other variables are defined by (21). However, we can simply use the general expression for  $\tau_w$  in terms of the wall viscosity  $\mu_w$  (20). In that case the blending of the velocity defined by (30) is used, and not the blending of the limiting wall shear stress values. The a priori evaluation of  $\tau_w^+$  for a plane channel, given in Fig. 7, shows the blending using Kader’s expression to be superior both to (26) and (27). Although the normalisation with  $u_\tau^+$  looks more convincing in Fig. 7, for practical reasons the  $u_k$  normalisation is always used in practice.

**Kinetic energy production** Computations with a sufficiently fine mesh in the near-wall region should reproduce correctly both the turbulent stress and the velocity gradient, which in turn should give a correct profile of  $\mathcal{P}$ , as illustrated for the plane channel flow in Fig. 9 with dashed lines (DNS  $Re_\tau = 800$ , [21]). When the coarse mesh is used, however, neither the turbulent stress nor the velocity gradient can be obtained correctly. Therefore in the standard wall function approach the value of  $\mathcal{P}$  is imposed assuming local equilibrium conditions: logarithmic velocity profile and constant shear stress. This gives a simple relation  $\mathcal{P} = u_\tau^3 / (\kappa y)$  (dash-dotted lines in Fig. 9), but it is correct only in the fully turbulent region in equilibrium flows.

Once we have an analytical expression for the velocity distribution across the near-wall region, we can derive an expression for  $\mathcal{P}$  by taking  $(\partial U / \partial y)$  obtained from (30) in combination with the near-wall and fully turbulent expressions for the turbulent

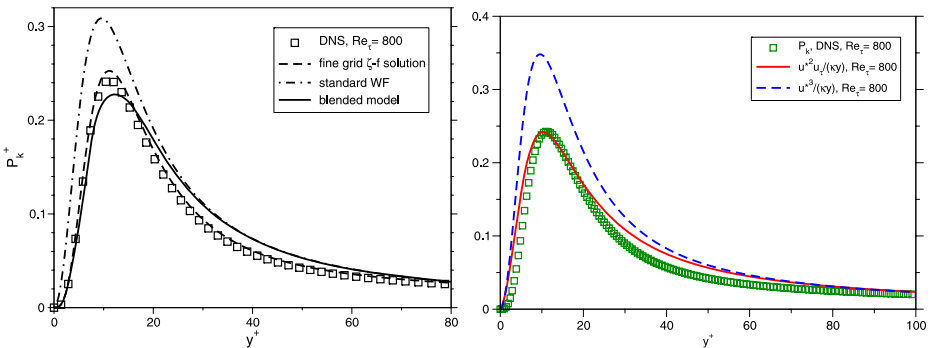


**Fig. 9** A priori evaluation of the blending expressions for the kinetic energy production  $\mathcal{P}$ , (34) (left) and of different expressions for  $\mathcal{P}$  ( $\mathcal{P} = u_k^3 / \kappa y$  and  $\mathcal{P} = u_\tau^2 u_\tau / \kappa y$ ) (right) Symbols: DNS of Tanahashi et al. [21]

stress. This, basically, reduces to the blending according to (32), where  $\phi_v$  here is the fine-resolution  $\mathcal{P}$  value from the integration to the wall, and  $\phi_t$  is the coarse-mesh  $\mathcal{P}$  from the WF approach:

$$\mathcal{P}_P = -\overline{uv} \frac{\partial U}{\partial y} = C_\mu^\zeta \xi_P \frac{k_P^2}{\varepsilon_P} \left( \frac{\partial U}{\partial y} \right)_P^2 e^{-\Gamma} + \frac{C_\mu^{3/4} k_P^{3/2}}{\psi_{PK} y_P} e^{-1/\Gamma} \tag{34}$$

Note that  $C_\mu^\zeta = 0.22$  and  $C_\mu = 0.07$ . Fig. 9 shows  $\mathcal{P}$  from (34), compared with the integration to the wall and the wall function approaches.

Figure 9 shows  $\mathcal{P}$  from (34), compared with the ItW and WF approaches. It is interesting to note that the standard practice in WF approach to compute  $\mathcal{P}$  from the log-law expression discussed above, but with  $u_\tau$  replaced by  $u_k = C_\mu^{1/4} k^{1/2}$  i.e.  $\mathcal{P} = u_k^3/\kappa y$  produces also a large over-prediction, even larger than the standard expression  $u_\tau^3/\kappa y$ , Fig. 9. This can be much improved when a combined velocity scale is applied, i.e. by  $\mathcal{P} = u_k^2 u_\tau/\kappa y$ , as illustrated in Fig. 9.

Other combination of the velocity scale, including also  $u_\zeta = C_\mu^{1/4} k^{1/2} \sqrt{\zeta/0.4}$ , can be used when solving the  $\zeta$ - $f$  to achieve similarly good agreement. However, while such a simple expression for  $\mathcal{P}$  may look more appealing for industrial computations than the blending expression (34), it is very doubtful that it would be valid in any other flows apart from the wall-attached equilibrium ones.

**Energy dissipation rate** We recall first that the kinetic energy dissipation rate  $\varepsilon$  satisfies the following expressions in the viscous sublayer (wall limit) and in the fully turbulent wall region, respectively:

$$\varepsilon_v = \frac{2\nu k}{y^2} \qquad \varepsilon_t = \frac{C_\mu^{3/4} k^{3/2}}{\kappa y} \tag{35}$$

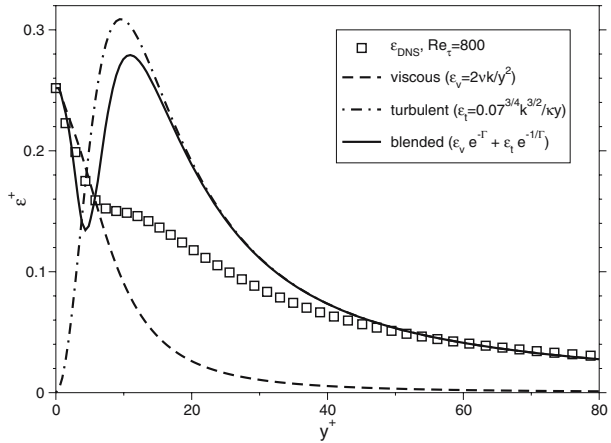
where again the subscripts “v” and “t” denote the viscous and fully turbulent values. We could now use the same blending (32) to express  $\varepsilon$  in the whole wall region. However, because of a very steep and specific (non-monotonic) variation of  $\varepsilon$  in the near-wall region, we found it beneficial to modify slightly the coefficient in the exponent of the blending function  $\Gamma$  (here denoted as  $\Gamma_\varepsilon$ ), so that the recommended expression for the complete near-wall region reads:

$$\varepsilon_P = \frac{2\nu k_P}{y_P^2} e^{-\Gamma_\varepsilon} + \frac{c_\mu^{3/4} k_P^{3/2}}{\kappa y_P} e^{-1/\Gamma_\varepsilon} \tag{36}$$

where  $\Gamma_\varepsilon = 0.001 y^{+4}/(1 + y^+)$ , and “P” denotes the values at the first near-wall grid node. Figure 10 shows a plot of (35) and (36) compared with the DNS results for a plane channel flow at  $Re_\tau = 800$ .

It is noted, however, that for the turbulent region  $\varepsilon_t$  is tied to  $\mathcal{P}_t$  and that even the simpler model (27) performs reasonably well. Despite satisfying the wall limit and the fully turbulent expressions, the blended curve shows a large discrepancy from the DNS data in the buffer region. One can improve agreement by further tuning of the blending functions, or even simply by reducing the value of the coefficient  $C_\mu$ . In the framework of the  $\zeta$ - $f$  (or any other model that provides the wall-normal stress component  $\overline{v^2}$  up to the wall, e.g.  $v^2$ - $f$  or a near-wall Reynolds stress model), one can utilise a striking similarity (at least in the channel flow) of the  $\mathcal{P}/\varepsilon$  and of  $\overline{uv^2}/(\overline{v^2}k)$  and deduce  $\varepsilon$  from  $\varepsilon = C_\mu \mathcal{P} \overline{v^2} k / \overline{uv^2}$ . While reproducing more accurately

**Fig. 10** A priori evaluation of the blended expressions for  $\varepsilon$ , (36) for a channel flow. Symbols: DNS of Tanahashi et al. [21]



$\varepsilon$  in the whole wall region, such an approach showed to cause numerical instabilities in most non-equilibrium flows tested (Popovac [15]).

However, we recall that it is not the local values of  $\mathcal{P}$  and  $\varepsilon$ , but their average over the cell, what is used as a boundary condition at the grid node P in the common finite-volume approach. Figure 11 shows a priori plots, using the DNS data, that the averaged kinetic energy production and dissipation rate,  $\overline{\mathcal{P}}$  and  $\overline{\varepsilon}$  agree very well for  $y^+ > 10$ . The major difference in the region  $y^+ < 10$  and the small difference above  $y^+ = 10$  is accounted for by the viscous contribution and blending functions in expressions for both quantities, (34) and (36) different.

**Elliptic relaxation function** For this function, none of the blending formulations (26), (27) or (32) is adequate for the CWT, for two reasons. First, the wall-limit (“viscous”) value of  $f$  ( $f^v = -2\nu\zeta\rho/y_p^2$ ) and its homogeneous value ( $f^t = (C_1 - 1 + C_2\mathcal{P}/\varepsilon)(\zeta - 2/3)/\tau$ ) have opposite signs. Second, while  $f^v$  ranges from its wall (negative) value to zero,  $f^t$  ranges from (positive) infinity to its homogeneous value (tends to zero). Thus there is a huge difference between them in the buffer region, and no blending (except the full elliptic solution) can give a realistic solution there.

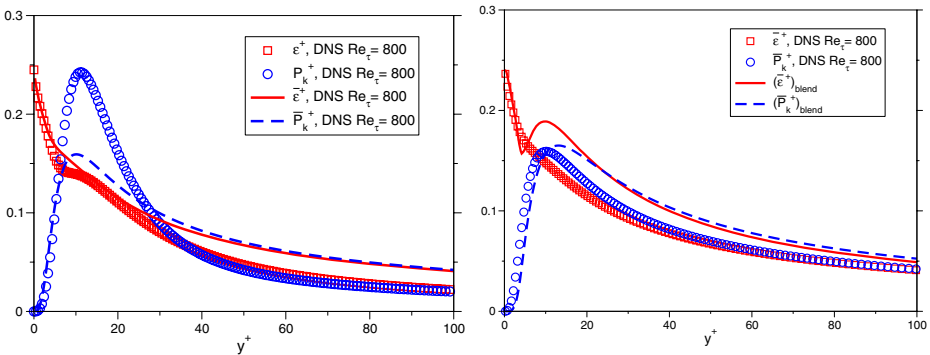


**Fig. 11** A priori evaluation of the cell-averaged production  $\overline{\mathcal{P}}$  and dissipation  $\overline{\varepsilon}$ , and their blended values  $\overline{\mathcal{P}}_{blend}$  and  $\overline{\varepsilon}_{blend}$ . Symbols: DNS of Tanahashi et al. [21]

Therefore, the simplest CWT for  $f$  is to manage its boundary condition in the same manner as for the standard  $\zeta$ - $f$  model with integration to the wall, i.e. to impose the wall value  $f_w$  obtained from the budget of (2):

$$f_w = \frac{-2\nu\xi_P}{y_P^2} \quad (37)$$

This definition is correct if the near-wall cell is in the viscous sublayer, and it gives zero value for  $f_w$  (it drops fast to zero, because of the power two in the denominator) away from the wall, which is incorrect. But since (37) sets only the boundary condition at the wall, the  $f$  equations will produce some approximate solution for the near-wall cell centre, due to in-domain flow conditions. This is acceptable because the wall blocking effect (which  $f$  should describe) fades away in the far-field.

## 5 Model Validation and Illustrations

As an illustration of the compound wall treatment (CWT) performance, we present some results of the computations of several generic flows including heat transfer with computational grids in which the wall-nearest grid node is placed in the buffer region. These computations are compared with the fine-grid integration up to the wall (ItW) using the  $\zeta$ - $f$  model, and, in some cases, with the generalised wall functions (GWF). Considered test cases include steady and pulsating plane channel flows, a round impinging jet and a separating flow behind a backward facing step. Apart from illustrating the performance of the near-wall treatment under different flow conditions, the aim was to check to what extent the results will deteriorate when the mesh is coarsen while keeping all other parameters the same.

**Steady and pulsating channel flow** For a steady plane channel flow, the computations were performed using several different meshes in which the first near-wall grid node was placed at  $y_P^+ = 0.05, 1, 10, 20$  and  $40$ . For all mesh sizes Fig. 12 shows that the obtained profiles of the velocity and the turbulent quantities agree very well with the reference data. The most notable difference between the reference and the here computed results is a kink in the turbulent shear stress between the first and the second point in the coarse mesh calculation (when  $y_P^+ = 40$ ). This is the typical outcome of all WF approaches because of the assumption that that near-wall turbulent shear stress is equal to the wall shear stress and this “aesthetic” anomaly is more pronounced at lower Re numbers.

In order to demonstrate the action of the non-equilibrium function  $\psi$ , (16) in conjunction with the CWT, we consider first the effect of flow unsteadiness in the computation of a pulsating turbulent channel flow. This is accounted for through the unsteady term  $\partial U/\partial t$  in the definition of  $C_U$ , (17). The results for  $Re_\tau = 350$  are compared with the LES by Scotti and Piomelli [24], Fig. 13.

For this case the near-wall treatment is very important, because during a pulsating cycle the local flow conditions near the wall (and consequently the wall shear stress, Fig. 13) are not following the regular sinusoidal variation of the centreline velocity, showing a deformation in the time curve and also a notable phase shift. While the velocity in the centreline shows not much sensitivity to the non-equilibrium function  $\psi$ , the inclusion of the unsteadiness in the CWT provides significant improvement

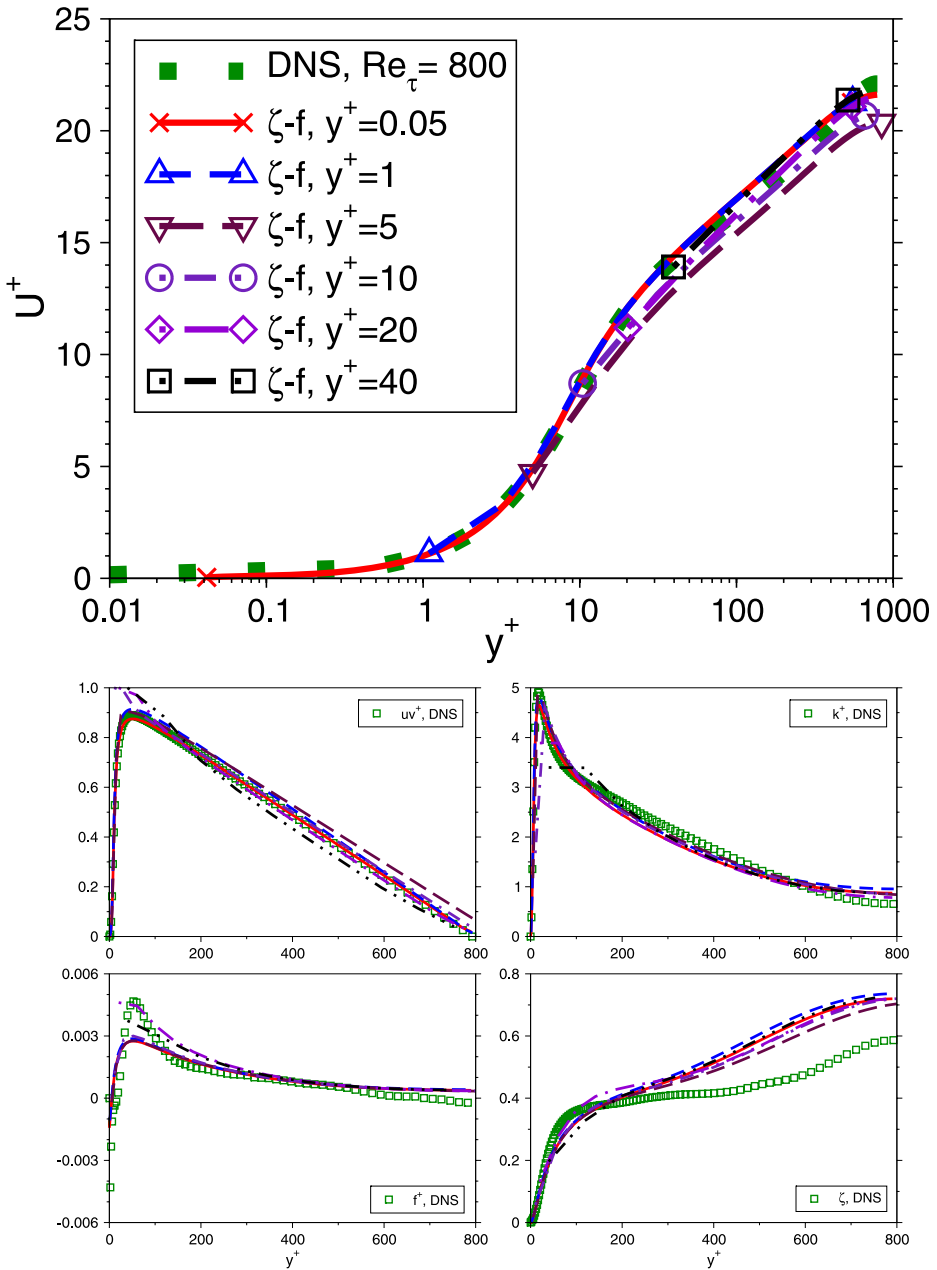


**Fig. 12** Results for  $U^+$ ,  $k^+$ ,  $\overline{uv}^+$ ,  $\zeta$  and  $f^+$  in the channel flow at  $Re_\tau = 800$ , computed on different grids with the first  $y^+_b$  ranging from 0.05 to 40. Symbols: DNS of Tanahashi et al. [21]

in reproducing the non-sinusoidal cyclic variation of the wall shear stress, Fig. 13, and of the maximum phase averaged shear stress and kinetic energy, Fig. 14. The inclusion of  $\psi$  from (16) predicts the negative minimum value of  $\tau_w$  in accord with the reference LES, whereas in the absence of  $\psi$  there is no mechanism that could give

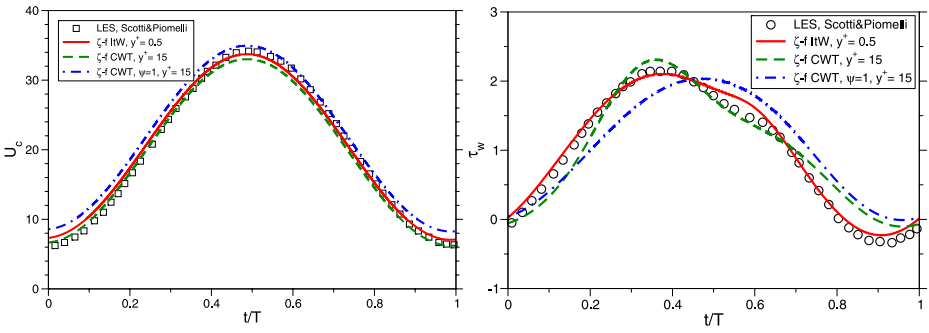


**Fig. 13** The time variation of the centreline velocity (*left*) and the wall shear stress (*right*) for the pulsating channel flow  $Re_\tau = 350$ . Symbols: LES of Scotti and Piomelli [24]

negative  $\tau_w$ . Another effect of  $\psi$  is the phase shift of the peak in the phase-averaged time variation of the turbulent shear stress and kinetic energy, which is qualitative in accord with the LES results, in contrast to more symmetric variation for  $\psi = 1$ .

**Round impinging jet** Impinging jet have long been regarded as a notorious challenge for RANS models especially when high-Re-number models are used in conjunction with wall functions. We considered a round jet at  $Re = 23,000$  and nozzle-to-plate distance  $H = 2D$ , which has been known to exhibit non-monotonic Nusselt number distribution with two peaks. The Nusselt number and friction factor on the target plate are given in Fig. 15, obtained both with and without the non-equilibrium function  $\psi$ .

The main challenge in impinging jets is the stagnation region where most turbulence models fail, but equally challenging is the prediction of the wall jet evolution, especially in round geometries where a strong adverse pressure gradient and consequent flow deceleration occur due to radial spreading of the wall jet. Proper accounting for these non-equilibrium effect is crucial for obtaining the correct behaviour (at least qualitatively) of the Nusselt number, which is evident

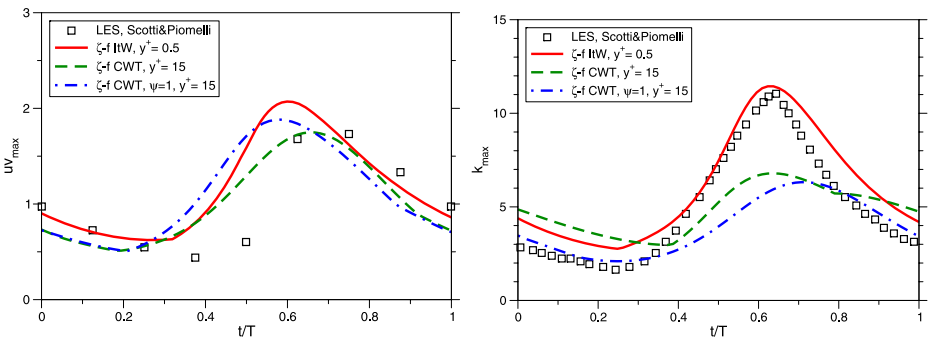


**Fig. 14** The time series of the maximum phase-averaged Reynolds shear stress (*left*) and the maximum phase-averaged turbulent kinetic energy (*right*) for the pulsating channel flow  $Re_\tau = 350$ . Symbols: LES of Scotti and Piomelli [24]

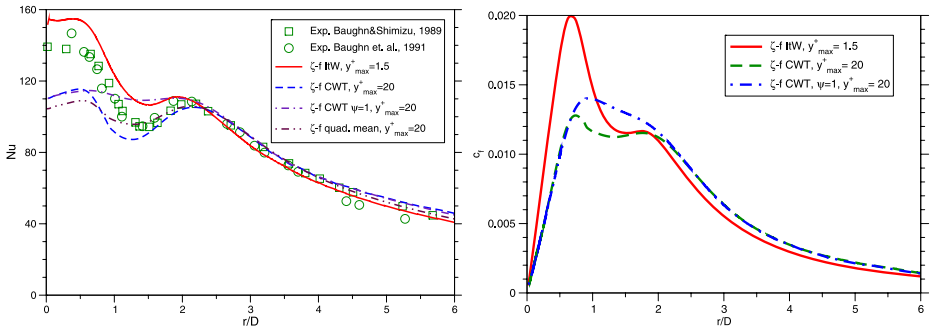


**Fig. 15** Distribution of the Nusselt number (*left*) and of the friction factor (*right*) along the impingement plate obtained with the  $\zeta$ - $f$  ItW and CWT models. Symbols: experiments of Baughn et al. [27] and Baughn and Shimizu [26]

from Fig. 15. Figure shows that the best reproduction of the experimental data is achieved with a proper integration up to the wall using a fine mesh resolution, but excluding some shortcomings in the stagnation zone, the Nusselt number seems well reproduced with the CWT using a coarse mesh with the wall-nearest grid node on average at  $y^+ \approx 20$ .

Velocity profiles at various radial positions proved also to be rather insensitive to the first grid node placement, as illustrated in Fig. 16, showing the magnitude of the velocity vector  $|U| = \sqrt{U^2 + V^2}$ .

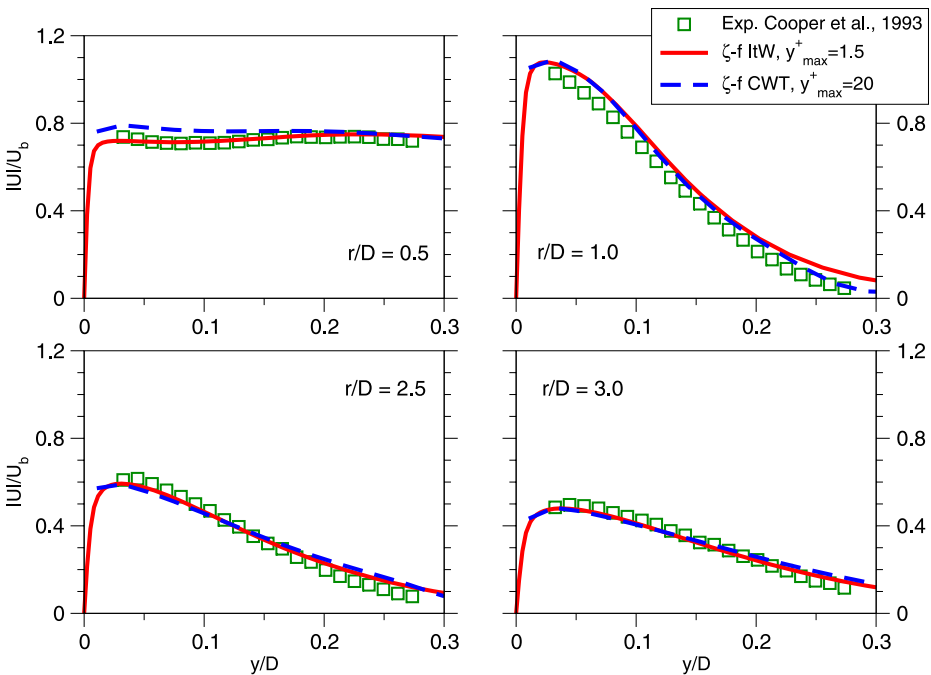


**Fig. 16** Velocity profiles in the impinging jet at various radial distances with a fine grid (ItW) and a coarse grid (CWT). Symbols: experiments of Cooper et al. [23]

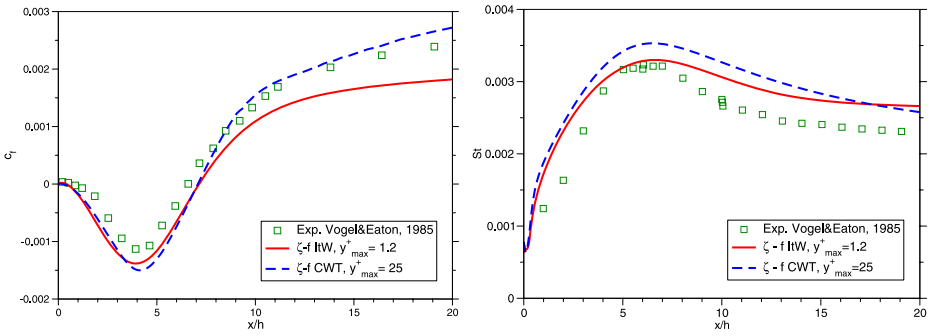


**Fig. 17** The distribution of the friction factor (*left*) and the Stanton number (*right*) along the backward facing step. Symbols: experiments of Vogel and Eaton [25]

**Backward-facing step flow** For testing the CWT approach in separating flows, we considered a flow behind a backward facing step at two Reynolds numbers:  $Re = 5,000$  and  $Re = 28,000$ , based on the step height. We present here some results for the latter case, which includes heat transfer, that was investigated experimentally by Vogel and Eaton [25]. The distribution of the friction factor and Stanton number along the wall behind the step, computed with ItW and CWT approach are shown in Fig. 17.

Slightly better results for the Stanton number and the friction factor are obtained with the non-equilibrium terms included than with  $\psi = 1$ , but the improvement is

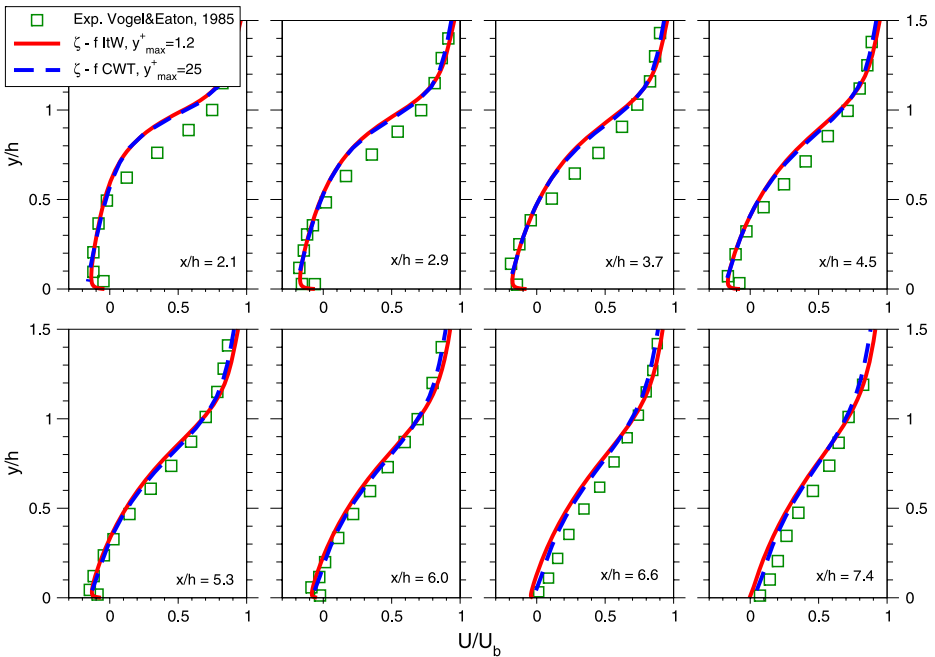


**Fig. 18** Velocity profiles behind a backward-facing step obtained with a *fine grid* (ItW) and a *coarse grid* (CWT). Symbols: experiments of Vogel and Eaton (1985) [25]

less pronounced than in the impinging jet case. This is because the backward facing step flow is much dominated by the shear layer enveloping the separation bubble and the overall pressure distribution, hence, the near-wall interventions cannot influence much the overall flow pattern. This is in contrast with the impinging jet, where capturing of the near-wall effects reflects directly on the prediction of the transition from the stagnation to the wall jet region.

Figure 18 shows velocity profiles at several cross-sections in the separation zone, close to reattachment and just behind it. Good agreement has been achieved at all locations between the solutions with the fine-grid ItW using the  $\zeta$ - $f$  model and with the CWT approach using a relatively coarse grid.

## 6 Conclusions

Recognising that the treatment of the wall boundary conditions in computations of turbulent flows and heat transfer still remains one of the weakest point in industrial CFD, we developed a compound wall treatment (CWT), which makes it possible to provide adequate boundary conditions in complex non-equilibrium flows irrespective of whether the wall-nearest grid node lies in the viscous sublayer, fully turbulent wall zone, or in the buffer region in between. The CWT combines a near-wall model designed for the integration up to the wall (ItW) with the wall function approach (WF) using Kader's blending functions. In principle (depending on the turbulence models used), all variables for which the wall boundary conditions are needed, can be treated in the same manner, simplifying thus the implementation of the CWT approach into any CFD code.

Although any near-wall model can be combined with any wall functions, for the ItW we opted for the robust elliptic-relaxation  $\zeta$ - $f$  eddy-viscosity model [8], which proved to reproduce a number of generic test flows as well as several complex industrial flows in excellent agreement with the available experimental or DNS results. Likewise, instead of the conventional wall functions that were derived under a number of assumptions – all implying energy-equilibrium conditions, we propose their generalisation (GWF) that makes the WFs applicable to non-equilibrium and transient flows. Both, the a priori and a posteriori testing of the GWFs in several non-equilibrium flows showed notable improvements as compared with the standard WFs.

The testing of the CWT in several generic flows without and with heat transfer, which include steady and pulsating flows in a plane channel, in a round impinging jet, and behind a backward-facing step, using different grids with the first node placed in the viscous sublayer, buffer zone or in the fully turbulent wall-region, all showed acceptable to good agreement with the available reference data. Subsequent testing of the GWT in several complex industrial flows, such as flow in the cylinder, through valves and in the cooling jacket of an IC engine ([22, 28]), in a mixer and in flow around a vehicle (in progress), all showed that the CWT approach is very robust and provides improvements as compared with the conventional WF approach. The CWT is especially suited for CFD of flows in complex configurations where the computational grid is generated automatically when it is usually difficult to achieve a priori the desired grid clustering that will satisfy either the ItW or WF prerequisites in the whole flow domain.

A word of caution warrants here concerning the computational mesh used for the CWT. While the use of relatively coarse meshes has always appealed, especially to industrial users of CFD, one should keep in mind that a coarse mesh gives less accurate calculation of gradients, and this can deteriorate the computational accuracy. In some cases it can also lead to numerical instabilities. Therefore, the wall function approach will sometimes require lower under-relaxation factors and more stable (but often slower) preconditioners and solvers. On the other hand, finer mesh computations will certainly give better results since the compound wall treatment will be approaching the full integration up to the wall, which is definitely more accurate than any pre-integrated wall function.

We close this section with a note regarding the issue of consistency of the wall boundary conditions with the full model equations solved in the outer flow region, raised by Kalitzin et al. [5]. It is noted that the here presented GWFs for velocity and temperature are consistent with the outer model (account for convection, pressure gradient and other source terms) when the first near-wall grid node lies in the fully turbulent region. And so are the boundary conditions for all variables when the first grid point lies very close to the wall within the viscous sublayer. In the intermediate (buffer) region, this consistency is not fully ensured because the expressions containing blending functions may not satisfy exactly the full model equations. But this deficiency is pertinent to most known wall treatments, (including the standard wall functions and various blending methods), and seems unavoidable if the procedure of defining wall boundary conditions is to be simple, computationally robust, and easily incorporable into existing CFD codes. Wall treatment in form of wall functions is an approximation in which a compromise is sought between the simplicity and robustness on one side and the overall quality of performance in a variety of complex flows using different computational grids.

**Acknowledgement** This work is a spin-off of the research project ENK6-CT-2001-00530 “Minimisation of NO<sub>x</sub> emission” (MinNO<sub>x</sub>), sponsored by the Research Directorate-General of the European Commission under the 5th Framework. The first-listed author (M.P.) acknowledges the financial support received from this project.

## References

1. Chieng, C.C., Launder, B.E.: On the calculation of turbulent heat transport downstream from an abrupt pipe expansion. *Numer. Heat Transf.* **3**, 189–207 (1980)
2. Craft, T.J., Gerasimov, A.V., Iacovides, H., Launder, B.E.: Progress in the generalisation of wall-function treatments. *Int. J. Heat Fluid Flow* **23**, 148–160 (2002)
3. Jayatilke, C.L.V.: The influence of Prandtl number and surface roughness on the resistance of the laminar sublayer to momentum and heat transfer. *Prog. Heat Mass Transf.* **1**, 193 (1969)
4. Esch, T., Menter, F.R.: Heat transfer predictions based on two-equation turbulence models with advanced wall treatment. *Turbul. Heat Mass Transf.* **4**, 633–640 (2003)
5. Kalitzin, G., Medic, G., Iaccarino, G., Durbin, P.: Near-wall behaviour of RANS turbulence models and implications for wall functions. *J. Comput. Phys.* **204**, 265–291 (2005)
6. Craft, T.J., Gant, S.E., Iacovides, H., Launder, B.E.: A new wall function strategy for complex turbulent flows. *Numer. Heat Transf., Part B* **45**, 301–317 (2004)
7. Kader, B.A.: Temperature and concentration profiles in fully turbulent boundary layers. *Int. J. Heat Mass Transfer* **24**, 1541–1544 (1981)
8. Hanjalic, K., Popovac, M., Hadziabdic, M.: A robust near-wall elliptic-relaxation eddy-viscosity turbulence model for CFD. *Int. J. Heat Fluid Flow* **25**, 1047–1051 (2004)
9. Durbin, P.A.: Near-wall turbulence closure modelling without ‘damping functions’. *Theor. Comput. Fluid Dyn.* **3**, 1–13 (1991)

10. Speziale, C.G., Sarkar, S., Gatski, T.: Modelling the pressure-strain correlation of turbulence: an invariant system dynamic approach. *J. Fluid Mech.* **227**, 245–272 (1991)
11. Laurence, D.R., Uribe, J.C., Utyuzhnikov, S.V.: A robust formulation of the  $v_2$ - $f$  model. *Flow Turbul. Combust.* **73**, 169–185 (2005)
12. Hanjalić, K., Laurence, D., Popovac, M., Uribe, C.: ( $v_2/k - f$ ) turbulence model and its application to forced and natural convection. In: Rodi, W., Mulas, M. (eds.) *Engineering Turbulence Modelling and Experiments*, vol. 6, pp. 67–76. Elsevier, Amsterdam, The Netherlands (2005)
13. Durbin P.A.: On the  $k-\epsilon$  stagnation-point anomaly. *Int. J. Heat Fluid Flow* **17**, 89–90 (1996)
14. Ng, E.Y.K., Tan, H.Y., Lim, H.N., Choi, D.: Near-wall function for turbulence closure models. *Comput. Mech.* **29**, 178–181 (2002)
15. Popovac, M.: Ph.D. thesis, Delft University of Technology, Delft, The Netherlands (2006)
16. Reichardt, H.: Vollstaendige Darstellung der turbulenten Geschwindigkeitsverteilung in glatten Leitungen. *ZAMM* **31**, 208–219 (1951)
17. Spalding, D.B.: A single formula for the law of the wall. *ASME J. Appl. Mech.* **28**, 444–458 (1961)
18. Musker, A.J.: Explicit expression for the smooth wall velocity distribution in a turbulent boundary layer. *AIAA J.* **17**, 655–657 (1979)
19. Liakopoulos, A.: Explicit representations of the complete velocity profile in a turbulent boundary layer. *AIAA J.* **22**, 844–846 (1984)
20. Shih, T., Povinelli, L., Liu, N.: Application of generalised wall functions for complex turbulent flows. In: Rodi, W., Fueyo, N. (eds.) *Engineering Turbulence Modelling and Experiments*, vol. 5, pp. 177–186. Elsevier, Amsterdam, The Netherlands (2002)
21. Tanahashi, M., Kang, S.-J., Miyamoto, S., Shiokawa, S., Miyauchi, T.: Scaling law of fine scale eddies in turbulent channel flows up to  $Re_\tau = 800$ . *Int. J. Heat Fluid Flow* **25**, 331–340 (2004)
22. Brohmer, A., Mehring, J., Scheider, J., Basara, B., Tatschl, R., Hanajlic, K., Popovac, M.: Progress in the 3D-CFD calculation of gas- and water-side heat transfer in IC-Engines. In: Eichlseder, H. (ed.) *10. Tagung der Arbeitsprozess der Verbrennungsmotors*, Technische Universität Graz, Austria, 22–23 September 2005
23. Cooper, D., Jackson, D.C., Launder, B.E., Liao, G.X.: Impinging jet studies for turbulence model assessment – I. Flow-filed experiments. *Int. J. Heat Mass Transfer* **36**, 2675–2684 (1993)
24. Scotti, A., Piomelli, U.: Numerical simulation of pulsating turbulent channel flow. *Phys. Fluids* **13**, 1367–1384 (2001)
25. Vogel, J.C., Eaton, J.K.: Combined heat transfer and fluid dynamic measurements downstream of a backward-facing step. *ASME J. Heat Transfer* **107**, 922–929 (1985)
26. Baughn, J., Shimizu, S.: Heat transfer measurements from a surface with uniform heat flux and an impinging jet. *ASME J. Heat Transfer* **111**, 1096–1098 (1989)
27. Baughn, J., Hechanova, W.E., Yan, X.: An experimental study of entrainment effects on the heat transfer from a flat surface to a heated circular impinging jet. *ASME J. Heat Transfer* **113**, 1023–1025 (1991)
28. Tatschl, R., Basara, B., Schneider, J., Hanjalic, K., Popovac, M., Brohmer, A., Mehring, J.: Advanced turbulent heat transfer modeling for IC-engine applications using AVL FIRE. In: *Int. Multidimensional Engine Modelling, User's Group Meeting*, Detroit, MI, 2 April 2006